Res Chem Intermed
https://doi.org/10.1007/s11164-018-3361-9

Synthesis and characterization of crude hydrotalcite Mg–Al–CO_3: study of thymol adsorption

Hamid Ziyat[1] · Mohammed Naciri Bennani[1] · Hassan Hajjaj[2] · Soumia Mekdad[1] · Omar Qabaqous[1]

Received: 7 October 2017 / Accepted: 1 March 2018

Abstract The study of the adsorption of thymol on a hydrotalcite of synthesis $Mg_3Al–CO_3$ (HT3) of molar ratio Mg/Al = 3 and on its counterpart enabled at 500 °C (HT3-C) was conducted in hexane at a concentration of 40 mg L^{-1} of thymol. Hydrotalcite HT3 was prepared via coprecipitation at a constant pH of 10 and characterized by X-ray diffraction, infrared spectroscopy, nitrogen adsorption–desorption methods and thermal analysis (TGA/DTA). The adsorption of the thymol tests were monitored by UV–visible spectroscopy. The results show that the calcined hydrotalcite (HT3-C) has a capacity of adsorption of thymol (8 mg g^{-1}) much greater than that of HT3 (4 mg g^{-1}), and the experimental points are described by the isotherm model of the Freundlich of both materials.

Keywords Layered double hydroxide LDH · Hydrotalcite · Adsorption · Thymol

✉ Hamid Ziyat
ziyat.hamid@gmail.com

✉ Mohammed Naciri Bennani
mbennanin@gmail.com

Hassan Hajjaj
h_hajjaj@yahoo.com

[1] Laboratory of Chemistry-Biology Applied to the Environment, Research Team "Applied Materials and Catalyses" Chemistry Department, Faculty of Sciences, Moulay-Ismail University, B.P. 11201, Zitoune, Meknes, Morocco

[2] Laboratory of Plant Biotechnology and Molecular Biology, Applied Mycology Team, Faculty of Sciences, Moulay-Ismail University, B.P. 11201, Zitoune, Meknes, Morocco

Published online: 16 March 2018

Introduction

The hydrotalcite is an anionic clay of the family of layered double hydroxides (LDHs). This latter constitutes an important class of layered ionic solids of general formula: $[\mathbf{M}^{2+}_{1-x}\mathbf{M}^{3+}_{x}(\mathbf{OH})_2]^{x+}[(\mathbf{A}^{n-})_{x/n} \cdot \mathbf{mH_2O}]^{x-}$, where, M^{2+} is a divalent cation (Mg^{2+}, Zn^{2+}, Ni^{2+}, Mn^{2+}, Fe^{2+},…), M^{3+} is a trivalent cation (Al^{3+}, Cr^{3+}, Fe^{3+}, Co^{3+}, Mn^{3+},…), A^{n-} represents the compensator anion (Cl^-, NO_3^-, CO_3^{2-},…), m is the number of water molecules interfolliaires, n denotes the load of the anion and x (= $M^{3+}/(M^{2+}+M^{3+})$) represents the charge density of the layers [1–3].

The LDHs and the mixed oxides resulting from their calcination have been found in many industrial applications thanks to the electrochemical and catalytic properties, exchanges and anionic of adsorbents [4]. These materials are used as a support of the active principles of certain drugs in the pharmaceutical field [5]; they can also be used as antibiotics because these materials are not toxic [6]. Previous studies have shown that anionic clays such as the layered double hydroxides are very interesting as adsorbents for heavy metals and other organic pollutants. Especially, their mixed metal oxides obtained after activation at 500 °C, which are characterized by high specific surfaces [7–16].

Essential oils or their active compounds are used as a protective agents against phytopathogenic fungi [17] and microorganisms invading foodstuffs [18]. Unlike chemicals such as pesticides and fertilizers they can be used as insecticides, as they do not adversely effect the environment or the consumer [19, 20]. Naturally occurring substances, and more particularly essential oils, currently offer an alternative solution for the protection of stored foodstuffs. However, their volatility poses a major problem in their use and the duration of their activity is very short. Thus, to remedy this problem and to prolong their effectiveness, several researchers have been interested in testing formulations based on essential oils and clay as a support for the storage of grains [21–24] and thus offer an alternative to conventional chemical agents, which have adverse effects on the environment. They can also be used as additives to feed poultry and ruminants to act as growth promoters and reduce the risk of the infection and the risk of the mycotoxin poisoning [25].

Thymol is a phenolic monoterpene, isolated from thyme. It is used for its antiseptic, antibacterial and antifungal properties [26] and in pharmaceuticals [27]. The aim of our work is the using a formulations based on natural substances and hydrotalcite or other materials for antifungal activity and other applications. In order to develop a formulations based on the thymol and the hydrotalcite, firstly, we are interested to study the kinetics of adsorption of the thymol on the hydrotalcite and its counterpart enabled at 500 °C to determine their relative adsorption capacity and to specify the kinetic model from the adsorption isotherms.

Materials and methods

Materials

The reagents used in this study are:

The metal salts ($MgCl_2$, $6H_2O$) and ($AlCl_3$, $6H_2O$) with a content of 99%, sodium hydroxide (NaOH) in pellet form with a purity of 98% and sodium carbonate (Na_2CO_3) with a purity of 99.9%, were provided by Loba Chemie. Hexane (C_6h_{14}) of purity > 85% and thymol of purity > 99% were respectively supplied by Loba Chemie and Sigma-Aldrich.

Characterization methods

Uncalcined and calcined hydrotalcite obtained were characterized by physico-chemical techniques (XRD, FTIR, BET, DTA/TGA).

X-ray powder diffraction analyses were carried out using a Philips PW 1800 (copper Kα radiation λ = 1.5418 Å, 40 kV, 20 mA). The spectra of the various samples were recorded in a range 2θ between 5° and 70° with an angular increment of 0.04°.

Fourier transform infrared spectra (FTIR) were obtained by using a JASCO 4000 Fourier transform spectrometer, equipped with a detector (TGS) and a ceramic source, separated by an optical system using an interferometer of Michelson. The samples (3% in KBr) were conditioned in pellets of 12 mm diameter. Absorption spectra were recorded in the range of 400 and 4000 cm^{-1} with a resolution of 4 cm^{-1}.

Textural analyses were performed by the BET method employing a Micromeritics ASAP 2010. The samples were previously degassed at 100 °C under vacuum overnight.

Thermogravimetric (TGA-DTA) analysis was carried out using Shimadzu TA-60 type apparatus, operating under air with a linear heating rate of 10 °C min^{-1} from ambient temperature to 600 °C.

Synthesis of hydrotalcite HT3 (Mg–Al–CO_3)

Hydrotalcite HT3 was prepared by the co-precipitation method at a constant pH [1]. This method consists simultaneously to precipitating two aqueous solutions. The first solution containing a mixture of the chloride salts of the divalent metal $MgCl_2$,$6H_2O$ (60.99 g) and chlorides of the trivalent element $AlCl_3$ (13.34 g) dissolved in 300 mL of distilled water, are defined by a molar ratio Mg/Al = 3. The second solution containing 2.12 g of the sodium carbonate (Na_2CO_3) and 32 g of the sodium hydroxide (NaOH) in 300 mL of distilled water. These two solutions were added dropwise while maintaining the pH at a basic value (pH = 10). The addition was carried out at ambient temperature under magnetic stirring. When the coprecipitation reaction was completed the resulting mixture is refluxed at 65 °C with stirring overnight to allow the growth of crystals. Then, the mixture was cooled

to room temperature, the precipitate was filtered by centrifugation and the solid obtained was washed several times with warm distilled water until a complete elimination of excess ions (Cl^-, Na^+). Then, dried in an oven at 75 °C overnight and then ground in a mortar, the material obtained is denoted HT3. The solid HT3 is calcined at a temperature of 500 °C. The calcination was carried out in a tubular furnace under air, overnight, according to a rise in temperature of 5 °C min^{-1}, the resulting solid is denoted HT3-C.

Kinetics and isotherm of adsorption of thymol on HT3 and HT3-C

The adsorption experiments were carried out in closed bottles with an absence of the light. To this effect, 50 mg of HT3 or HT3-C with 10 mL solution of thymol diluted in hexane (initial concentration C_0 = 40 mg L^{-1}). The mixtures were stirred at room temperature (4500 rpm), and the kinetics of the adsorption of thymol on various solids was measured at a regular times t_{ads} (30 min, 1, 2, 4, 6, 8 and 15 h). After each time t_{ads}, the mixture is separated by centrifugation at 3400 rpm for 8 min before analysis. Then, the supernatant is analyzed by UV–Vis spectroscopy, and the residual concentration was determined by measuring the absorbance at the wavelength of 273 nm. The amount of thymol adsorbed at equilibrium (q_e, in mg g^{-1}) was calculated using the following equation [28]:

$$q_e = \frac{(C_0 - C_e) * V}{m} \quad (1)$$

where C_0 and C_e are the initial and the equilibrium concentration of the thymol (mg L^{-1}), respectively. m is the mass of adsorbent (g); V is the volume (mL) of thymol solution and q_e (mg g^{-1}) is the adsorbed amount per gram of adsorbent.

The adsorption isotherms were carried out under the same conditions as those of the adsorption kinetics using an increasing concentration of thymol from 0 to 130 mg L^{-1}. The contents of the vials were stirred for 5 h until the equilibrium time was reached and then centrifuged. The residual concentrations and the adsorbed amounts were determined as previously (Eq. 1).

Theoretical background

In this part, we present the expressions used to describe the kinetic of the studied models.

Modelling of adsorption kinetics

Pseudo-first-order kinetics The expression of the pseudo-first-order kinetics model [29–31] is given by the equation:

$$\ln(q_e - q_t) = \ln q_e - K_1 * t \quad (2)$$

where q_e is the amount adsorbed at the equilibrium per gram of adsorbent (mg g^{-1}).

q_t is the amount adsorbed at a given time t (mg g^{-1}). t represents the contact time (min) and K_1 is the adsorption rate constant for the first-order adsorption (min^{-1}).

By plotting ln ($q_e - q_t$) versus the time t, we can determine the adsorption rate constant K_1 and the adsorbed amount at the equilibrium q_e.

Pseudo-second-order kinetics The kinetics model of the pseudo-second order [30, 32] is expressed by the equation:

$$\frac{t}{q_t} = \frac{1}{K_2 * q_e^2} + \frac{t}{q_e} \tag{3}$$

where K_2 is the rate constant for the pseudo second order (g mg^{-1} min^{-1}) and q_e is the amount of thymol adsorbed at the equilibrium (mg g^{-1}).

The quantity adsorbed at the equilibrium (q_e) and the constant K_2 can be determined experimentally from the slope and the ordinate at the origin of the right $\frac{t}{q_t}$ versus t.

The intra-particle diffusion model The intra-particle diffusion model was proposed by Weber and Morris [33, 34]. This model is used to determine the limiting step in the adsorption mechanism. The expression of this model is expressed by the equation:

$$q_t = K_d * t^{0.5} + C \tag{4}$$

where K_d is the intraparticle diffusion constant in (mg g^{-1} $min^{-1/2}$) and C is a constant, which characterizes the diffusion of the solute in the liquid phase. The values of K_d and C are deduced from the slope and the ordinate at the origin of Eq. (4).

Adsorption isotherms

Langmuir model The Langmuir model [35, 36] is given by the following equation:

$$\frac{q_e}{q_{max}} = \frac{(K_L * C_e)}{(1 + K_L * C_e)} \tag{5}$$

The linear form of Langmuir equation (Eq. 5) is:

$$\frac{1}{q_e} = \frac{1}{C_e} * \frac{1}{(q_{max} * K_L)} + \frac{1}{q_{max}} \tag{6}$$

where q_e is the equilibrium adsorbed amount (mg g^{-1}); C_e is the equilibrium concentration (mg L^{-1}); K_L is the Langmuir equilibrium constant (L mg^{-1}) and q_{max} is the quantity maximum adsorption (mg g^{-1}).

Another parameter without dimension, called the separation factor (R_L) whose expression is given by the equation:

$$R_L = \frac{1}{1 + K_L * C_0} \tag{7}$$

where C_0 is the initial concentration of the adsorbate (mg L^{-1}) and K_L (L mg^{-1}) is the Langmuir constant.

Depending on the value R_L defined by Hall et al. [37, 38], this parameter allows predicting if the Langmuir model is favorable or not. If $0 < R_L < 1$, the isotherm is favorable; if $R_L = 1$, the isotherm is linear; if $R_L > 1$, the isotherm is not favorable and if $R_L = 0$, the isotherm is irreversible [37, 39].

Freundlich model The Freundlich model [36, 40] is given by the empirical formula:

$$q_e = K_F * C_e^{1/n} \tag{8}$$

The commonly used form is the linear form, which gives equation:

$$\ln q_e = \ln K_F + \frac{1}{n} \ln C_e \tag{9}$$

where q_e is the concentration of the adsorbate (mg g^{-1}); C_e is often expressed in mg L^{-1}; K_F is a constant relative to the adsorption capacity; n is the constant relative to the affinity between the adsorbate and the surface, whereas $n = 1$ corresponds to a chemical adsorption process and $n > 1$ corresponds to a physical adsorption mechanism.

Results and discussion

Physico-chemical characterization of HT3 and HT3-C

XRD analysis

The X-ray diffractograms of HT3 and HT3-C are shown in Fig. 1. The pattern of the uncalcined solid is typical of a pure and well crystallized hydrotalcite compound and characteristic of a hexagonal network with rhombohedral symmetry (space group: R-3m). The pattern shows the existence of the family lines (00l), which are intense and symmetrical to the low values of two theta encountered in the hydrotalcite compounds [2, 41, 42].

The reticular distances of the peaks (003) and (110) allow calculation of the parameters **a** and **c** of HT3. The interreticular distances of the peak (110) located toward 60° in 2θ represents the half metal–metal distance in the sheet and the interreticular distances of the peak (003) located toward 11° at 2θ corresponds to the interfeuillet distance. The hexagonal mesh parameters are calculated from the relations a = 2d(110) and c = 3d(003) according to Bragg law. The mesh parameters of the solid hydrotalcite are summarized in Table 1. These results are in agreement with those found in the literature [7, 43].

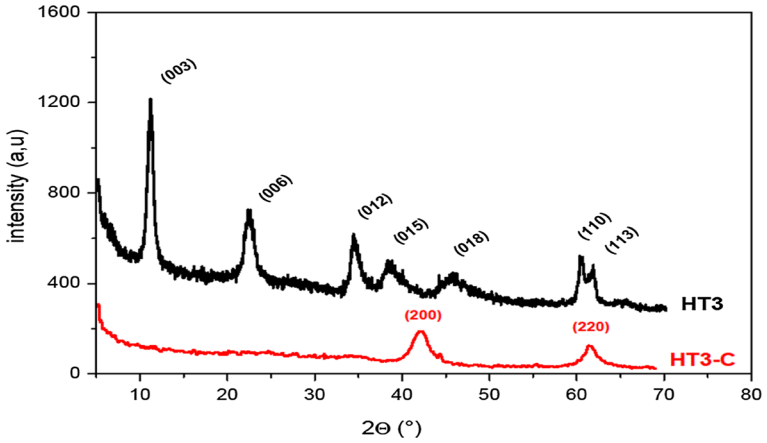

Fig. 1 X-ray diffraction patterns of HT3 and HT3-C

Table 1 The parameters mesh of HT3

Sample	d_{003} (Å)	d_{110} (Å)	a (Å)	c (Å)
HT3	7.86	1.53	3.06	23.58

From Fig. 1, the X-ray pattern of the compound calcined at 500 °C (HT3-C) shows the disappearance of the different characteristic peaks of the layered structure and the appearance of the two new broad peaks (200) and (220) correspond the mixed oxide of the magnesium and the aluminum [44].

FTIR analysis

The infra-red spectra of calcined HT3 and HT3 are shown in Fig. 2.

Before calcination of HT3, the infra-red spectrum shows a characteristic band of LDH with the carbonate anions intercalated in the interlayer space [45]. The spectrum of HT3 shows a broad absorption band at 3480 cm^{-1} , which corresponds to the O–H stretching vibration of the layered hydroxide groups bound to the various metals (M–OH, M = Al or Mg) and to the valence vibrations of the O–H groups of the water physisorbed on the surface and to the water molecules inserted in the interlayer space. A band around 1640 cm^{-1} is also observed, corresponding to the bending vibration mode of the interlayer water. The band toward 1370 cm^{-1} is attributed to the anti-symmetric stretching vibration of C–O, indicating the existence of the carbonate anions $\nu(CO_3^{-2})$ of the inter-walled space [44]. The bands that appear around 600–650 cm^{-1} and at about 400–450 cm^{-1} are attributed to the metal–oxygen ν(M–O) and oxygen–metal–oxygen ν(O–M–O) vibrations, respectively. These bands are characterized of the band LDHs [16, 46, 47]. It is also noted that the IR spectrum of calcined hydrotalcite at 500 °C is similar to the HT3

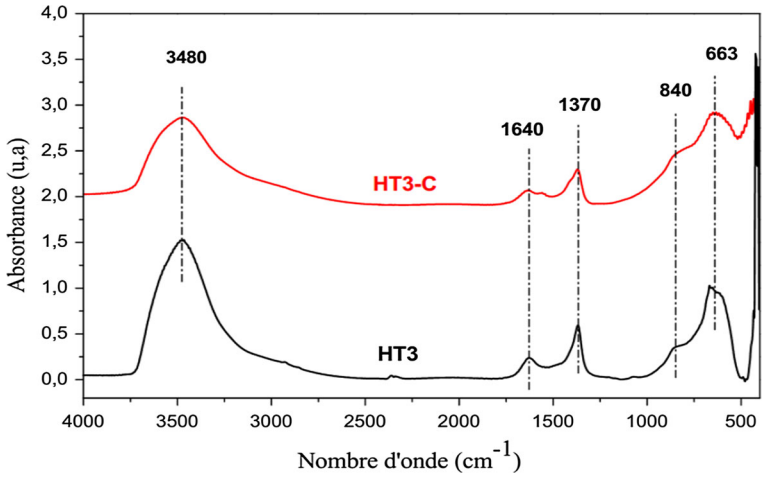

Fig. 2 FTIR spectra of various samples HT3 and HT3-C

spectrum, but with a marked decrease in the intensity of the bands appearing at about 3480 and 1640 cm^{-1}; these results are due to the departure of the water molecules intercalated in the sheets. The band toward 1370 cm^{-1} becomes broad and decreases significantly in intensity, reflecting a partial decomposition of the carbonates of the hydrotalcite. These observations are in agreement with the DTA/TGA results presented in Fig. 3.

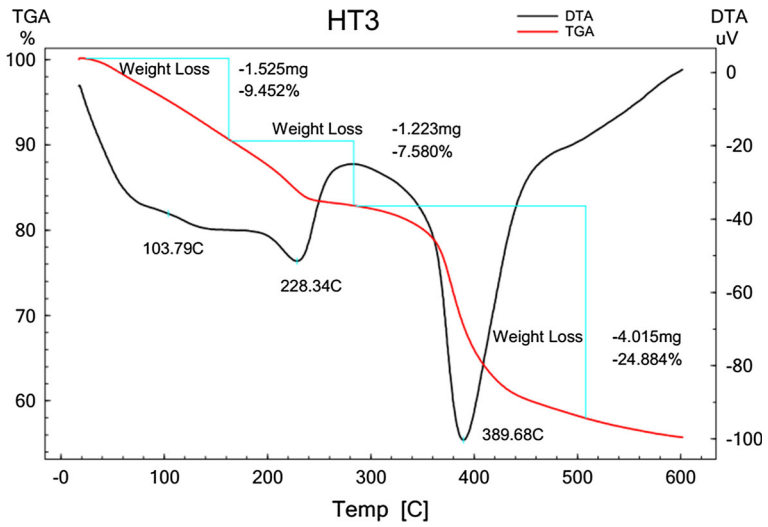

Fig. 3 DTA and TGA plots of HT3

Thermal analysis DTA/TGA

The results of the DTA/TGA analysis plotted in Fig. 3 show that the decomposition of uncalcined HT3 takes place according to three distinct endothermic steps corresponding to three mass losses: A first loss of mass around 103 °C on the order of 10% occurs due to the departure of water molecules weakly bound or adsorbed on the outer faces of the crystals. A second mass loss of 7.58%, of which the maximum is at 228 °C, corresponds to the loss of the intercalated water molecules. The third loss of mass is almost 24.88% between 300 and 500 °C, attributed to the beginning of the decomposition of the carbonate compensating anions and the dehydroxylation of the layers [16]. The total mass loss at 600 °C is equal to 42%.

BET analysis

The specific surfaces areas of HT3 and HT3-C of the solids are given in Table 2:

It is noted that the calcination of the hydrotalcite (Table 2) provoked a significant increase in its specific surface area, it passes from 52 to 139 $m^2\ g^{-1}$ following activation at 500 °C as is generally known in the literature and as observed by Stošić et al. [48] in the case of LDH materials. This result is explained by the fact that during the calcination step, the solid undergoes phenomena of dehydration, dehydroxylation and decarboxylation of the structure as previously observed by XRD, FTIR and DTA/TGA; that is to say formation of the mixed oxide of Mg and Al.

Adsorption studies of thymol on HT3 and HT3-C

Adsorption kinetics

Figure 4 shows the quantities of thymol adsorbed on HT3 and HT3-C versus time. The curves obtained show that the adsorption kinetics of thymol on both adsorbents are relatively rapid at the beginning of the process and stabilize after 4 h of contact. This rapid climb, more pronounced in the case of HT3-C, it is due to the availability of the active sites at the beginning of the adsorption process. At the equilibrium, the quantities of the thymol adsorbed of HT3 and HT3-C are of the order of 4 and 8 mg g^{-1}, respectively, for an initial concentration of 40 mg L^{-1}.

Notice that, whatever the type of adsorbent, equilibrium of the adsorption is reached after 4 h of the contact. Subsequently, a contact time of 5 h was chosen for the determination of the adsorption isotherms.

Table 2 Specific surface area determined by the BET method of HT3 and HT3-C

Sample	Specific surface area ($m^2\ g^{-1}$)
HT3	52
HT3-C (500 °C)	139

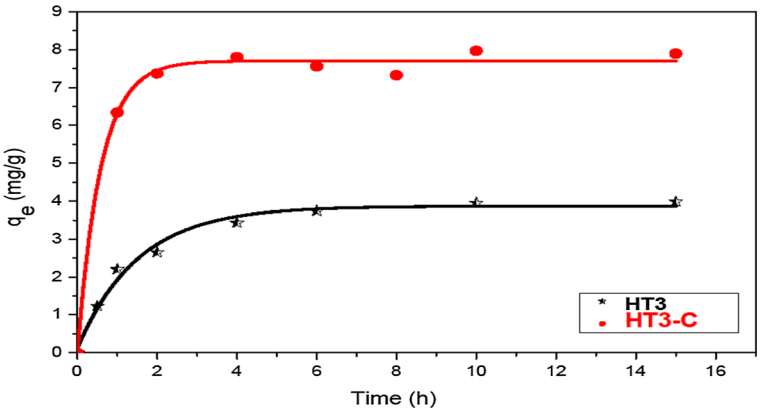

Fig. 4 Adsorption kinetic plots of thymol on the HT3 and HT3-C

The plots of ln $(q_e - q_t)$ and $\frac{t}{q_t}$ as a function of the time (respectively, Eqs. 2, 3) are given in Fig. 5a, b.

It is seen that the adsorption of thymol on the two solids HT3 and HT3-C perfectly follows a pseudo-second-order model (Fig. 5b). This is confirmed by the fact that the values of the adsorbed quantities (q_e) determined by this model are close to those obtained experimentally (q_{exp}), and the correlation coefficients are very close to 1 ($R^2 = 0.99$) (Table 3). Similar results have been obtained by Ngeumchouin et al. in the study of the adsorption of terpene compounds on homosodiques and modified clays [49]. Ho and McKay have also observed that the most adsorption reactions on solid materials obey pseudo-second-order kinetics [30].

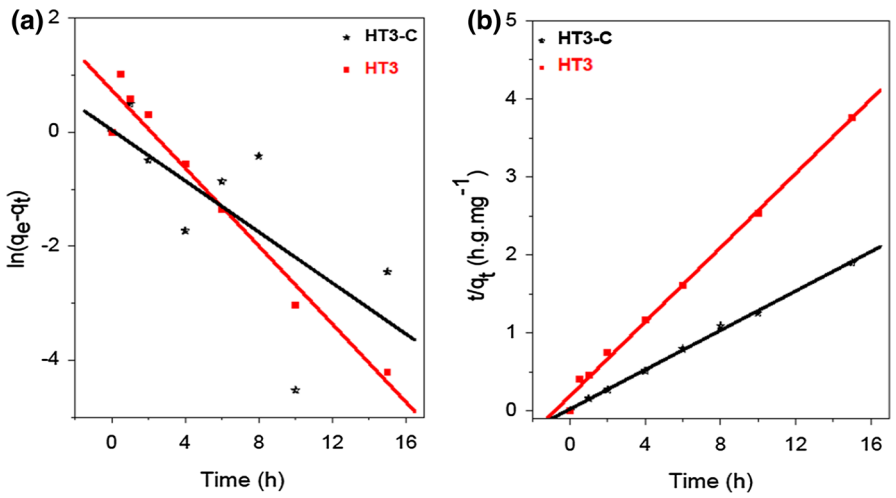

Fig. 5 Linear representation of the kinetic model of thymol adsorption on HT3 and HT3-C: Pseudo-fist-order model (**a**) and Pseudo-second-order model (**b**)

Table 3 Kinetic parameters for thymol adsorption on the HT3 and HT3-C

Sample	q_{exp} (mg g^{-1})	Lagergren (Pseudo-first-order model)			Ho et al. (Pseudo-second-order model)		
		q_e (mg g^{-1})	K_1	R^2	q_e	K_2	R^2
HT3	4	2.09	0.34	0.98	4.21	0.30	0.99
HT3-C	7.98	1.04	0.22	0.70	7.93	0.71	0.99

q_{exp} and q_e in mg g^{-1}; K_1 in min^{-1}; K_2 in g mg^{-1} min^{-1}

In Fig. 6, the representation of q_t versus the square root of the time ($t^{1/2}$) gives two straight lines, which shows that the adsorption of thymol on HT3 and HT3-C takes place in two steps: The first step is rapid and probably corresponds to the transfer of thymol from the solution to the external surface of the adsorbent. The second step is characterized by a slow evolution towards the state of the equilibrium and it represents the adsorbent–adsorbate interaction. These results confirm an adsorption according to a kinetic of the pseudo-second-order.

Moreover, the values of the constant C are different from 0 (Table 4), which suggest that the intra-particle diffusion is not the only step that controls the rate of adsorption of thymol on HT3 and HT3-C, as observed by Ozcan et al., in the adsorption of blue 193 acid on DEDMA-sepiolite [50].

The quantity of the thymol adsorbed has been considerably increased in the case of HT3-C as a result of high specific surface area (139 m^2 g^{-1}: Table 2), following the heat treatment at 500 °C, which shows that the superficial properties, especially the number of adsorption sites, also have an influence on adsorption. Similar results were obtained by Arab et al. [9] and Bakhti et al. [51] in the study of the adsorption of Cr(VI) on a hydrotalcite Mg–Al–CO_3 calcined at T = 450 °C during 2 h and on a hydrotalcite Mg–Al–CO_3 and their homologous calcined at T = 550 °C, respectively.

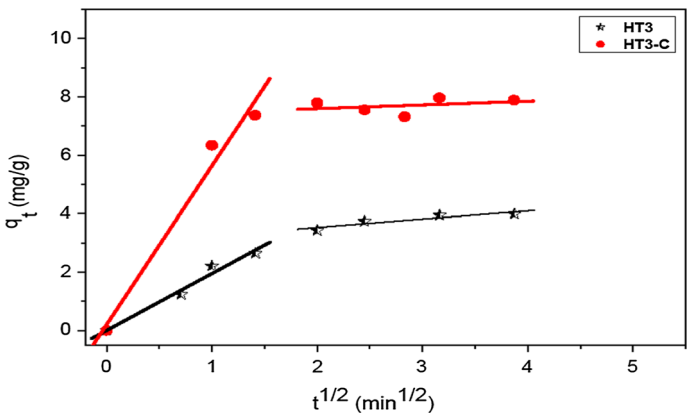

Fig. 6 Intra-particle diffusion plots for thymol adsorption onto HT3 and HT3-C

Table 4 Intraparticle diffusion parameters for the adsorption of thymol onto HT3 and HT3-C

K_{d1} and K_{d2} in (mg g^{-1} $min^{-1/2}$)

Samples	Step 1			Step 2		
	C	K_{d1}	R^2	C	K_{d2}	R^2
HT3	0.004	1.95	0.99	2.95	0.29	0.92
HT3-C	0.20	5.44	0.99	7.35	0.13	0.34

Adsorption isotherms

Figure 7 shows that the adsorption of the thymol increases with the increase of the initial thymol concentration. Similar results were obtained by Elmiz et al. [52] and by Ngeumchouin et al. [49] in the study of the adsorption of the thymol on homosodique bentonite and homosodique bentonite and modified by surfactants, respectively.

The adsorption isotherms of thymol were simulated by using the Langmuir and the Freundlich models. The linear transforms of the isotherms are shown in Fig. 8a, representing the Langmuir model, and Fig. 8b, representing Freundlich model.

It is observed that the experimental results coincide perfectly with the linear forms of the two models (Langmuir and Freundlich).

The values of K_L, n, q_{max}, K_F and the correlation coefficients for Langmuir and Freundlich models of HT3 and HT3-C are grouped in Table 5.

The values of R^2 are very close to 1 for the two solids HT3 and HT3-C in the case of both models (Table 5).

From Table 5, the calculated values of R_L for C_0 varying from 40 to 200 mg L^{-1} are located between 0 and 1 ($0 < R_L < 1$) for HT3 but for HT3-C are close to 0 and the adsorbed amount for HT3 is far to the value found experimentally. These results

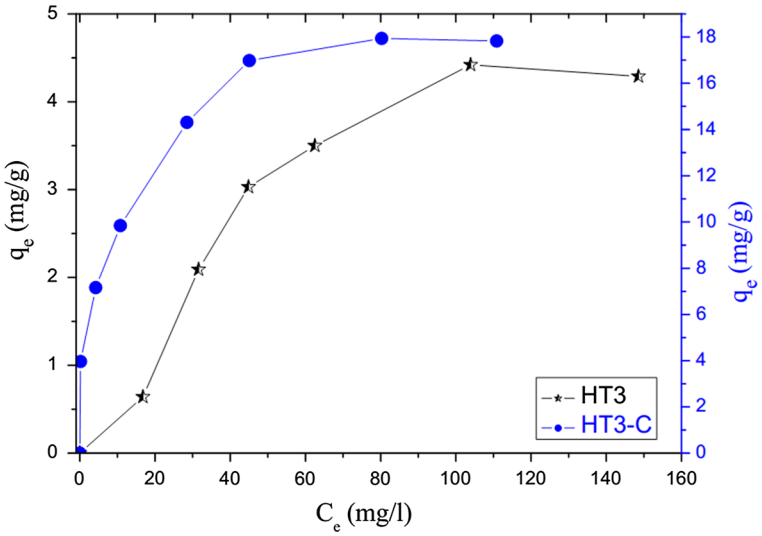

Fig. 7 Adsorption isotherms of thymol onto HT3 and HT3-C (m = 50 mg, V = 10 mL and t = 5 h)

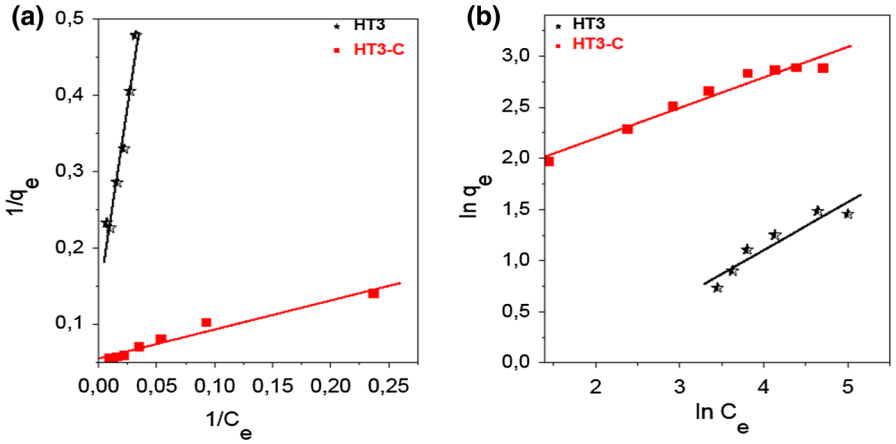

Fig. 8 Langmuir (**a**) and Freundlich (**b**) plots for adsorption of thymol onto HT3 and HT3-C

Table 5 Isotherm parameters for the adsorption of thymol onto HT3 and HT3-C

Sample	Langmuir				Freundlich		
	q_{max}	K_L	R_L	R^2	n	K_F	R^2
HT3	7.35	0.01	0.33–0.71	0.98	2.14	0.46	0.94
HT3-C	18.23	0.14	0.04–0.15	0.98	3.35	4.95	0.98

q_{max} in (mg g^{-1}), K_F in (mg g^{-1}) and K_L in (mg g^{-1})

allow predicting that the Langmuir model is not suitable to describe the adsorption phenomenon.

However, the K_F constants of the Freundlich model show in Table 5, indicating a strong adsorption capacity for HT3 and HT3-C. It is also found that the value of n greater than 1 is envisaged for a physical adsorption process, in agreement with the results of Tsai et al., who studied the effect of the particle size of the activated clay on the adsorption of paraquat [53]. To this effect, the Freundlich model seems well suited and shows that the two materials, HT3 and HT3-C, present the sites of adsorption of thymol that are heterogeneous in nature. Moreover, it seems that the adsorption of thymol by the two materials follows the Freundlich model. That is to say the adsorption is done on a heterogeneous site surface during the adsorption of thymol on HT3 and HT3-C. Similar results have been reported by Ngeumchouin et al. during the study of thymol adsorption on modified clays by surfactants and by metals [49].

Conclusion

In this work, we are interested in the study of the adsorption of the thymol on a synthetic clay (hydrotalcite) and its counterpart enabled at 500 °C with the aim of considering later the development of clay-essential oil formulations. The results obtained show that:

- The hydrotalcite $MgAlCO_3$ of ratio Mg/Al = 3 used in this work was prepared via the coprecipitation method at constant pH. The characterization by XRD, FTIR and DTA/TGA has shown that the synthesized hydrotalcite presents a pure and well-crystallized phase.
- Thymol adsorption was carried out in the presence of the hexane under well-defined conditions with the synthesized hydrotalcite (HT3) and thermally activated at 500 °C (HT3-C).
- Both materials have a variable adsorption capacity of thymol. Thermal activation significantly improves the adsorption capacity, ranging from 4 mg g^{-1} for HT3 to 8 mg g^{-1} for HT3-C according experimental conditions. This increase is due in part to the increase in the specific surface area of the solid after calcination.
- The study of the adsorption kinetics of thymol on HT3 and HT3-C shows that the adsorption is carried out in two stages: the first step is rapid and the equilibrium is reached after 4 h of contact for the two materials, and the kinetics corresponds well to the pseudo-second-order model. Examination of the adsorption isotherms shows that the Freundlich model can perfectly describe the adsorption of the thymol.

References

1. W.T. Reichle, Solid State Ion. **22**, 135 (1986)
2. A.V.F. Cavani, F. Trifiro, Catal. Today **11**, 173 (1991)
3. A. Vanaamudan, B. Chavada, P. Padmaja, J. Environ. Chem. Eng. **4**, 2617 (2016)
4. A. Taguchi, F. Schuth, Microporous Mesoporous Mater. **77**, 1 (2005)
5. E. Manasse, Atti Della Soc. Toscana Di Sci. Nat. **24**, 92 (1915)
6. W.-Z. Li, J. Lu, J.-S. Chen, G.-D. Li, Y.-S. Jiang, L.-S. Li, B.-Q Huang, J. Chem. Technol. Biotechnol. **81**, 89 (2006)
7. Y. Lin, Q. Fang, B. Chen, J. Environ. Sci. China **26**, 493 (2014)
8. F. Yang, S. Sun, X. Chen, Y. Chang, F. Zha, Z. Lei, Appl. Clay Sci. **123**, 134 (2016)
9. L. Arab, M. Boutahala, B. Djellouli, C. R. Chim. **17**, 860 (2014)
10. C. Lei, X. Zhu, B. Zhu, C. Jiang, Y. Le, J. Yu, J. Hazard. Mater. **321**, 801 (2017)
11. T. Wang, Z. Cheng, B. Wang, W. Ma, Chem. Eng. J. **181–182**, 182 (2012)
12. Z.Q. Zhang, H.Y. Zeng, X.J. Liu, S. Xu, C.R. Chen, J.Z. Du, J. Taiwan Inst. Chem. Eng. **60**, 361 (2016)
13. L. Xiao, W. Ma, M. Han, Z. Cheng, J. Hazard. Mater. **186**, 690 (2011)
14. L. Deng, Z. Shi, X. Peng, S. Zhou, J. Alloys Compd. **688**, 101 (2016)
15. R.M.M. dos Santos, R.G.L. Gonçalves, V.R.L. Constantino, C.V. Santilli, P.D. Borges, J. Tronto, F.G. Pinto, Appl. Clay Sci. **140**, 132 (2017)
16. R. Extremera, I. Pavlovic, M.R. Pérez, C. Barriga, Chem. Eng. J. **213**, 392 (2012)

17. A. Zambonelli, A.Z. D'Aulerio, A. Severi, S. Benvenuti, L. Maggi, A. Bianchi, J. Essent. Oil Res. **16**, 69 (2004)
18. T. Mangena, N. Muyima, Lett. Appl. Microbiol. **28**, 291 (1999)
19. M.B. Isman, Annu. Rev. Entomol. **51**, 45 (2006)
20. B. Conti, A. Canale, P.L. Cioni, G. Flamini, Bull. Insectol. **63**, 197 (2010)
21. S.M. Kéita, C. Vincent, J.P. Schmit, J.T. Arnason, A. Bélanger, J. Stored Prod. Res. **37**, 339 (2001)
22. M.M.G. Nguemtchouin, M.B. Ngassoum, L.S.T. Ngamo, P.M. Mapongmetsem, J. Sieliechi, F. Malaisse, G.C. Lognay, E. Haubruge, T. Hance, Appl. Clay Sci. **44**, 1 (2009)
23. M.M.G. Nguemtchouin, M.B. Ngassoum, L.S.T. Ngamo, X. Gaudu, M. Cretin, Crop Prot. **29**, 985 (2010)
24. M.G.M. Nguemtchouin, M.B. Ngassoum, P. Chalier, R. Kamga, L.S.T. Ngamo, M. Cretin, J. Stored Prod. Res. **52**, 57 (2013)
25. A.R. Chami, Patent, Advanced Scientific Developments (2014)
26. N.V. Yanishlieva, E.M. Marinova, M.H. Gordon, V.G. Raneva, Food Chem. **64**, 59 (1999)
27. R.D. MacPherson, Anaesthesia **56**, 965 (2001)
28. Y. Huang, X. Ma, G. Liang, H. Yan, Chem. Eng. J. **141**, 1 (2008)
29. S. Lagergren, Handlingar **4**, 1 (1898)
30. Y.S. Ho, G. McKay, Chem. Eng. J. **70**, 115 (1998)
31. Y.S. Ho, Scientometrics **59**, 171 (2004)
32. Y.S. Ho, G. McKay, Process Biochem. **34**, 451 (1999)
33. G. McKay, V.J.P. Poots, J. Chem. Technol. Biotechnol. **30**, 279 (1980)
34. J.C. Weber, W.J. Morris, J. Sanit. Eng. Div. Am. Soc. Civ. Eng. **89**, 31 (1963)
35. I. Langmuir, J. Am. Chem. Soc. **40**, 1361 (1918)
36. G. Limousin, J.P. Gaudet, L. Charlet, S. Szenknect, V. Barthès, M. Krimissa, Appl. Geochem. **22**, 249 (2007)
37. K.R. Hall, L.C. Eagleton, A. Acrivos, T. Vermeulen, I&EC Fundam. **5**, 212 (1966)
38. W. Weber, R.K. Chakravorti, Am. Inst. Chem. Eng. J. **20**, 229 (1974)
39. G. Bayramoglu, B. Altintas, M.Y. Arica, Chem. Eng. J. **152**, 339 (2009)
40. H. M. Freundlich, J. Phys. Chem. **57**, 385 (1906)
41. T. Kameda, M. Saito, Y. Umetsu, J. Alloys Compd. **402**, 46 (2005)
42. J. Yu, J. Li, H. Wei, J. Zheng, H. Su, X. Wang, J. Mol. Catal. A: Chem. **395**, 128 (2014)
43. M. Naciri Bennani, D. Tichit, F. Figueras, S. Abouarnadasse, J. Chim. Phys. Phys. Chim. Biol. **96**, 498 (1999)
44. F. Bruna, R. Celis, M. Real, J. Cornejo, J. Hazard. Mater. **225–226**, 74 (2012)
45. M.J. Hernandez-Moreno, M.A. Ulibarri, J.L. Rendon, C.J. Serna, Phys. Chem. Miner. **12**, 34 (1985)
46. J.C.A.A. Roelofs, J.A. van Bokhoven, A.J. van Dillen, J.W. Geus, K.P. de Jong, Chem. A Eur. J. **8**, 5571 (2002)
47. S. Mekdad, M. Naciri Bennani, H. Ahlafi, J. Adv. Chem. **8**, 10 (2014)
48. D. Stošić, F. Hosoglu, S. Bennici, A. Travert, M. Capron, F. Dumeignil, J.-L. Couturier, J.-L. Dubois, A. Auroux, Catal. Commun. **89**, 14 (2017)
49. M.G.M. Nguemtchouin, M.B. Ngassoum, R. Kamga, S. Deabate, S. Lagerge, E. Gastaldi, P. Chalier, M. Cretin, Appl. Clay Sci. **104**, 110 (2015)
50. A.S. Özcan, B. Erdem, A. Özcan, J. Colloid Interface Sci. **280**, 44 (2004)
51. A. Bakhti, M.S. Ouali, Rev. Des Sci. L'eau **20**, 241 (2007)
52. M. El Miz, S. Salhi, I. Chraibi, A. El Bachiri, M. Fauconnier, A. Tahani, Open J. Phys. Chem. **4**, 98 (2014)
53. W.T. Tsai, C.W. Lai, K.J. Hsien, J. Colloid Interface Sci. **263**, 29 (2003)